HHS Public Access

Author manuscript

Science. Author manuscript; available in PMC 2016 October 15.

Published in final edited form as:

Science. 2016 April 15; 352(6283): 353–358. doi:10.1126/science.aad7297.

Nuclear envelope rupture and repair during cancer cell migration

Celine M. Denais[1,†], **Rachel M. Gilbert**[1,†], **Philipp Isermann**[1,†], **Alexandra L. McGregor**[1], **Mariska te Lindert**[2], **Bettina Weigelin**[2], **Patricia M. Davidson**[1], **Peter Friedl**[2,3,4], **Katarina Wolf**[2], and **Jan Lammerding**[1,*]

[1]Nancy E. and Peter C. Meinig School of Biomedical Engineering & Weill Institute for Cell and Molecular Biology; Cornell University; Ithaca, NY; USA [2]Department of Cell Biology; Radboud University Medical Center; Nijmegen, The Netherlands [3]Department of Genitourinary Medical Oncology, The University of Texas MD Anderson Cancer Center; Houston, TX; USA [4]Cancer Genomic Center, The Netherlands (CGC.nl)

Abstract

During cancer metastasis, tumor cells penetrate tissues through tight interstitial spaces, requiring extensive deformation of the cell and its nucleus. Here, we investigated tumor cell migration in confining microenvironments in vitro and in vivo. Nuclear deformation caused localized loss of nuclear envelope (NE) integrity, which led to the uncontrolled exchange of nucleo-cytoplasmic content, herniation of chromatin across the NE, and DNA damage. The incidence of NE rupture increased with cell confinement and with depletion of nuclear lamins, NE proteins that structurally support the nucleus. Cells restored NE integrity using components of the endosomal sorting complexes required for transport-III (ESCRT-III) machinery. Our findings indicate that cell migration incurs substantial physical stress on the NE and its content, requiring efficient NE and DNA damage repair for survival.

The nuclear envelope (NE), comprised of the inner and outer nuclear membranes, nuclear pore complexes, and the nuclear lamina, presents a physical barrier between the nuclear interior and the cytoplasm that protects the genome from cytoplasmic components and establishes a separate compartment for DNA and RNA synthesis and processing (1). Loss of NE integrity and nuclear pore selectivity have been linked to the normal aging process and a variety of human diseases, including cancer (2). In cancer progression, key steps of tumor cell invasion depend upon deformation of the nucleus into available spaces within the three-dimensional tissue (3–6). Whereas the cytoplasm of migrating cells can penetrate even submicron-sized pores, the deformation of the large and relatively rigid nucleus becomes a rate-limiting factor in migration through pores less than 25 μm^2 in cross-section (4, 6–10).

*Correspondence to: jan.lammerding@cornell.edu.
†Authors contributed equally.

Supplementary Materials:
Materials and Methods
Figures S1–S15
Movies S1–S7
References (*33–42*)

We hypothesized that migration through such tight spaces provides a substantial mechanical challenge to the integrity of the nucleus. Thus, we investigated whether cell migration through confining spaces induces NE rupture and compromises DNA integrity, and how cells repair such NE ruptures during interphase.

To model cancer cell invasion with precise control over cell confinement, we designed a microfluidic device containing constrictions with fixed height and varying widths mimicking interstitial pore sizes (Figs. S1A–B)(11). We detected NE rupture using previously established fluorescent reporters consisting of green or red fluorescent proteins fused to a nuclear localization sequence (NLS-GFP and NLS-RFP, respectively) that rapidly escape into the cytoplasm when NE integrity is lost (12–14). Breast cancer, fibrosarcoma, and human skin fibroblast cells displayed transient loss of NE integrity, coinciding with the nucleus passing through the constrictions (Figs. 1A–B, S1C–L; Movie S1). NE rupture was associated with transient influx of fluorescently labeled cytoplasmic proteins into the nucleus (Fig. S2) and could also be detected by accumulation of the fluorescently labeled DNA-binding proteins barrier-to-autointegration factor (BAF)(15) and cyclic GMP-AMP synthase (cGAS)(16) at sites of NE rupture (Fig. S3).

We then tested whether NE rupture also occurs during cancer cell migration in biological environments. Fibrosarcoma cells and skin fibroblasts exhibited NE rupture during migration in fibrillar collagen matrices (Figs. 1C–D, S4; Movie S2), with similar kinetics to those recorded in the constriction channels (Figs. S1M). NE rupture typically occurred when the minimal nuclear diameter, which closely matches the pore size encountered by the cell (6), dropped to 3 μm (Fig. 1D–E), thereby linking NE rupture to cell movement through narrow spaces. Accordingly, NE ruptures were rare (i.e., below 5% per ≈12 hour observation period) for cells migrating on glass, in low-density collagen matrices, or through 15 × 5 μm^2-wide channels, in line with previously reported rates of spontaneous NE rupture in cancer cell lines (13). However, when matrix pore sizes were reduced to below 5–20 μm^2 by increasing collagen concentration and/or blocking the cells' ability to cleave collagen fibers and widen pores by addition of a matrix metalloprotease (MMP) inhibitor, the incidence of NE rupture increased 10-fold and more (S5A–B). Similarly, reducing the pore size of the microfluidic channels to less than 20 μm^2 increased NE rupture more than 10-fold (S5C–D). Irrespective of the experimental model, the incidence of NE rupture increased exponentially with decreasing pore size (Fig. 1F) and reached over 90% when the nuclear height was confined to 3 μm (Fig. S5E). Imaging HT1080 fibrosarcoma cells invading into the collagen-rich mouse dermis in live tumors after orthotopic implantation confirmed that migration-induced NE rupture also occurs in vivo, particularly in individually disseminating cells (Figs. 1G–J, S6; Movie S3). NE rupture was less prevalent in cells moving as multicellular collective strands (Figs. 1J, S6), which typically follow linear tracks of least resistance and undergo less pronounced nuclear deformations (3, 7).

NE rupture in vitro and in vivo was often accompanied by protrusion of chromatin through the nuclear lamina (Figs. 2A–B, S7A-I; Movies S4–5). The incidence of such 'chromatin herniations' increased significantly with decreasing pore sizes (Figs. 2C, S7H). In severe cases, small pieces of the nucleus were pinched off from the primary nucleus as cells passed through narrow constrictions (Fig. 2D; Movie S6), resulting in an elevated and persistent

fraction of cells with fragmented nuclei (Fig. 2E, S7J). Furthermore, cells that had passed through microfluidic constrictions had more nuclear fragments positive for γ-H2AX, a marker of DNA double-strand breaks (17), than cells that had not yet entered the constrictions (Fig. 2F), consistent with recent reports that loss of NE integrity in micronuclei can cause DNA damage (14) and chromothripsis (18). Intense γ-H2AX staining could also be found at chromatin protrusions (Fig. S8A). To confirm that DNA damage was caused by migration-induced nuclear deformation and NE rupture, we performed live-cell imaging on cells co-expressing NLS-GFP and fluorescently labeled 53BP1 (RFP-53BP1), another marker of DNA damage (19, 20). NE rupture, and even severe nuclear deformation alone, resulted in rapid formation of new RFP-53BP1 foci as cells squeezed through the constrictions (Figs. 2G–H, S8B–G), consistent with previous reports of increased activation of DNA damage response genes after compression-induced chromatin herniation and NE rupture (21).

To gain further insights into the biophysical processes underlying NE rupture, we analyzed the timing and location of NE rupture in regard to nuclear deformation, local membrane curvature, NE composition, and cytoskeletal forces. NE rupture occurred predominantly (≈76%) at the leading edge of the nucleus (Fig. 3A–B) and was almost always (89.9 ± 2.14%, n = 198 cells) preceded by, or coincided with, the formation of nuclear membrane protrusions (‘blebs’) as the nuclei moved through the constrictions (Figs. 1C, 1H, 3A, 3C; S9). Nuclear membrane blebs typically (96.1 ± 1.38%, n = 178 blebs) formed at sites where the nuclear lamina signal, particularly the lamin B1 network, was weak or absent (Figs. 3D–F, S10A–B). These findings indicate that blebs form when segments of the nuclear membrane detach from the nuclear lamina and bulge into the cytoplasm. Depletion of lamins A/C and lamin B2 significantly increased the likelihood of NE rupture (Figs. 3G, S10C), which together with previous studies (4, 12,13, 21–23) suggest that lamins are important for stabilizing the NE.

Consistent with previous observations (13, 21,22, 24, 25), the expanding nuclear blebs were devoid of GFP-lamin B1 (Fig. 3D–F) and nuclear pores (Fig. S10D), and initially contained little, or no GFP-lamin A and B2 (Fig. S10A–B). Upon NE rupture the blebs retracted and collapsed (Figs. 1C, 1H, 3A, 3C, S9, S10E–H), suggesting that hydrostatic pressure was released from the fluid-filled blebs. Although the NE contains pores, recent studies demonstrated that the NE can provide an effective barrier to support intracellular pressure gradients (26, 27). Nuclear pressurization could arise from actomyosin contraction at the rear of the nucleus that is required to move the nucleus through tight spaces (5, 6), effectively mimicking cellular compression experiments (21, 22). Supporting this idea, treatment with low concentrations of blebbistatin, a myosin II inhibitor, significantly decreased the incidence of nuclear rupture (Fig. 3H) without inhibiting the ability of cells to migrate through larger channels (Fig. S10I)

The transient nature of NE rupture suggests that cells can efficiently restore nuclear membrane integrity during interphase. We observed rapid (<2 min) accumulation of GFP-lamin A at the site of rupture that correlated with the severity of nuclear rupture and that often persisted for hours (Figs. 3I–K, S11). Subsequent ruptures within the same cell occurred at distinct sites (Fig. S11A), implying local protection by these ‘lamin scars’. Two

recent reports identified that members of the ESCRT family are involved in re-sealing the nuclear membrane during late anaphase (28, 29). To assess whether ESCRT proteins have a similar function in interphase NE repair, we generated GFP-fusion constructs of the ESCRT-III subunit CHMP4B, involved in recruiting other ESCRT-III proteins and facilitating membrane scission, and the ESCRT-III–associated AAA-ATPase VPS4B, which is required for disassembly and recycling of ESCRT-III proteins (30). Upon NE rupture induced by confined migration or laser ablation, CHMP4B-GFP and VPS4B-GFP rapidly (≤2 min) formed transient foci at the site of nuclear membrane damage (Figs. 4A–D, S12, S13A–C; Movie S7). Super-resolution microscopy confirmed recruitment of endogenous ESCRT-III proteins to sites of NE rupture into complexes ≤ 160 nm in size (Figs. 4E, S13D–H). Recruitment of the ESCRT-III machinery was independent of microtubules (Fig. S14). Depletion of the ESCRT-III subunit CHMP2A, CHMP7, or ectopic expression of a dominant-negative VPS4B mutant (GFP-VPS4B^{E235Q}) that prevents ESCRT-III subunit recycling, significantly increased the time required for nucleo-cytoplasmic re-compartmentalization (Figs. 4F–G, S13I–N), indicating a crucial role of ESCRT-III proteins in restoring nuclear membrane integrity. To assess the functional relevance of NE repair, we quantified cell viability after NE rupture. Under normal condition, the vast majority (>90%) of cells survived even repeated NE rupture (Fig. 1A, 4H, S4A). Inhibiting either ESCRT-III mediated NE repair or DNA damage repair pathways alone did not reduce cell viability, but inhibition of both NE and DNA repair substantially increased cell death after NE rupture (Fig. 4H).

Taken together, our studies demonstrate that cell migration through confining spaces, as frequently encountered during cancer cell invasion, can challenge the integrity of the NE and DNA content, which could promote DNA damage, aneuploidy and genomic rearrangements, and—in the absence of efficient repair—cell death. We propose a biophysical model in which cytoskeletal-generated nuclear pressure results in the formation and eventual rupture of nuclear membrane blebs at sites of high membrane curvature and weakness in the underlying nuclear lamina (Fig. S15). These events could be particularly prominent in cells with reduced levels of lamins, whose expression is deregulated in many cancers and often correlates with negative outcomes (31, 32). While NE rupture, and resulting genomic instability, may promote cancer progression, it may also represent a particular weakness of metastatic cancer cells and an opportunity to develop novel anti-metastatic drugs by specifically targeting these cells, for example, by blocking NE repair and inhibiting DNA damage repair.

Supplementary Material

Refer to Web version on PubMed Central for supplementary material.

Acknowledgments

The authors thank G. Lahav, A. Loewer, M. Zwerger, M. Smolka, S. Emr, N. Buchkovich, B. Burke, H. Worman, S. Young, L. Fong, D. Discher, J. Broers, J. Goedhart, H. Yu and W. Zipfel for cells, reagents, and helpful discussion. The authors acknowledge E. Wagena for mouse surgery and cell transfection, C. Paus for generation of in vitro collagen data, and K. Zhang, E. Ghazoul, D. Huang, G. Fedorchak, G.-J. Bakker and F. Ahmadpour for help with image analysis. The authors are grateful to M. Piel and colleagues for sharing their unpublished data and manuscript. This work was supported by awards from the National Institutes of Health (NIH) [R01 HL082792 and

R01 NS059348], the Department of Defense Breast Cancer Research Program [BC102152; BC BC150580], the National Science Foundation (NSF) [CBET-1254846], the National Cancer Institute through the Cornell Center on the Microenvironment & Metastasis [U54 CA143876], and an NSF Graduate Research Fellowship to A.L.M [DGE-1144153]. This work was further supported by the Netherlands Science Organization [NWO-VIDI 917.10.364 to K.W.; NWO-VICI 918.11.626 to P.F.] and the Cancer Genomics Center, Netherlands. This work was performed in part at the Cornell NanoScale Facility, which is supported by the NSF [Grant ECCS-15420819]. Imaging was performed in part through the Cornell University Biotechnology Resource Center, which is supported by NYSTEM [CO29155], NIH [S10OD018516], and NSF [1428922], and by the Radboud UMC Microscopic Imaging Center and the preclinical animal imaging center (PRIME). Additional experimental details and data are available in the Supplementary Materials.

References and Notes

1. Burke B, Stewart CL. Functional architecture of the cell's nucleus in development, aging, and disease. Current topics in developmental biology. 2014; 109:1. [PubMed: 24947235]
2. Hatch E, Hetzer M. Breaching the nuclear envelope in development and disease. The Journal of cell biology. 2014 Apr 28.205:133. [PubMed: 24751535]
3. Weigelin B, Bakker G-J, Friedl P. Intravital third harmonic generation microscopy of collective melanoma cell invasion. Principles of interface guidance and microvesicle dynamics. IntraVital. 2012; 1:32.
4. Harada T, et al. Nuclear lamin stiffness is a barrier to 3D migration, but softness can limit survival. The Journal of cell biology. 2014 Mar 3.204:669. [PubMed: 24567359]
5. Thomas DG, et al. Non-muscle myosin IIB is critical for nuclear translocation during 3D invasion. The Journal of cell biology. 2015 Aug 17.210:583. [PubMed: 26261182]
6. Wolf K, et al. Physical limits of cell migration: control by ECM space and nuclear deformation and tuning by proteolysis and traction force. The Journal of cell biology. 2013 Jun 24.201:1069. [PubMed: 23798731]
7. Friedl P, Wolf K, Lammerding J. Nuclear mechanics during cell migration. Current opinion in cell biology. 2011 Feb.23:55. [PubMed: 21109415]
8. Davidson PM, Denais C, Bakshi MC, Lammerding J. Nuclear deformability constitutes a rate-limiting step during cell migration in 3-D environments. Cell Mol Bioeng. 2014 Sep 1.7:293. [PubMed: 25436017]
9. Rowat AC, et al. Nuclear envelope composition determines the ability of neutrophil-type cells to passage through micron-scale constrictions. The Journal of biological chemistry. 2013 Mar 22.288:8610. [PubMed: 23355469]
10. Fu Y, Chin LK, Bourouina T, Liu AQ, VanDongen AM. Nuclear deformation during breast cancer cell transmigration. Lab on a chip. 2012 Oct 7.12:3774. [PubMed: 22864314]
11. Davidson PM, Sliz J, Isermann P, Denais C, Lammerding J. Design of a microfluidic device to quantify dynamic intra-nuclear deformation during cell migration through confining environments. Integrative biology : quantitative biosciences from nano to macro. 2015 Dec 30.7:1534. [PubMed: 26549481]
12. De Vos WH, et al. Repetitive disruptions of the nuclear envelope invoke temporary loss of cellular compartmentalization in laminopathies. Human molecular genetics. 2011 Nov 1.20:4175. [PubMed: 21831885]
13. Vargas JD, Hatch EM, Anderson DJ, Hetzer MW. Transient nuclear envelope rupturing during interphase in human cancer cells. Nucleus. 2012 Jan-Feb;3:88. [PubMed: 22567193]
14. Hatch EM, Fischer AH, Deerinck TJ, Hetzer MW. Catastrophic nuclear envelope collapse in cancer cell micronuclei. Cell. 2013 Jul 3.154:47. [PubMed: 23827674]
15. Jamin A, Wiebe MS. Barrier to Autointegration Factor (BANF1): interwoven roles in nuclear structure, genome integrity, innate immunity, stress responses and progeria. Current opinion in cell biology. 2015 Jun.34:61. [PubMed: 26072104]
16. Civril F, et al. Structural mechanism of cytosolic DNA sensing by cGAS. Nature. 2013 Jun 20.498:332. [PubMed: 23722159]

17. Nakamura AJ, Rao VA, Pommier Y, Bonner WM. The complexity of phosphorylated H2AX foci formation and DNA repair assembly at DNA double-strand breaks. Cell cycle. 2010 Jan 15.9:389. [PubMed: 20046100]
18. Zhang CZ, et al. Chromothripsis from DNA damage in micronuclei. Nature. 2015 Jun 11.522:179. [PubMed: 26017310]
19. Bekker-Jensen S, Lukas C, Melander F, Bartek J, Lukas J. Dynamic assembly and sustained retention of 53BP1 at the sites of DNA damage are controlled by Mdc1/NFBD1. The Journal of cell biology. 2005 Jul 18.170:201. [PubMed: 16009723]
20. Loewer A, Karanam K, Mock C, Lahav G. The p53 response in single cells is linearly correlated to the number of DNA breaks without a distinct threshold. BMC biology. 2013; 11:114. [PubMed: 24252182]
21. Le Berre M, Aubertin J, Piel M. Fine control of nuclear confinement identifies a threshold deformation leading to lamina rupture and induction of specific genes. Integrative biology : quantitative biosciences from nano to macro. 2012 Nov.4:1406. [PubMed: 23038068]
22. Broers JL, et al. Decreased mechanical stiffness in LMNA−/− cells is caused by defective nucleo-cytoskeletal integrity: implications for the development of laminopathies. Human molecular genetics. 2004 Nov 1.13:2567. [PubMed: 15367494]
23. Lammerding J, et al. Lamin A/C deficiency causes defective nuclear mechanics and mechanotransduction. The Journal of clinical investigation. 2004 Feb.113:370. [PubMed: 14755334]
24. Shimi T, et al. The A- and B-type nuclear lamin networks: microdomains involved in chromatin organization and transcription. Genes & development. 2008 Dec 15.22:3409. [PubMed: 19141474]
25. Shimi T, et al. Structural Organization of Nuclear Lamins A, C, B1 and B2 Revealed by Super-Resolution Microscopy. Molecular biology of the cell. 2015 Aug 26.
26. Petrie RJ, Koo H, Yamada KM. Generation of compartmentalized pressure by a nuclear piston governs cell motility in a 3D matrix. Science. 2014 Aug 29.345:1062. [PubMed: 25170155]
27. Neelam S, et al. Direct force probe reveals the mechanics of nuclear homeostasis in the mammalian cell. Proceedings of the National Academy of Sciences of the United States of America. 2015 May 5.112:5720. [PubMed: 25901323]
28. Olmos Y, Hodgson L, Mantell J, Verkade P, Carlton JG. ESCRT-III controls nuclear envelope reformation. Nature. 2015 Jun 11.522:236. [PubMed: 26040713]
29. Vietri M, et al. Spastin and ESCRT-III coordinate mitotic spindle disassembly and nuclear envelope sealing. Nature. 2015 Jun 11.522:231. [PubMed: 26040712]
30. Hurley JH. ESCRTs are everywhere. The EMBO journal. 2015 Oct 1.34:2398. [PubMed: 26311197]
31. Hutchison CJ. Do lamins influence disease progression in cancer? Advances in experimental medicine and biology. 2014; 773:593. [PubMed: 24563367]
32. Matsumoto A, et al. Global loss of a nuclear lamina component, lamin A/C, and LINC complex components SUN1, SUN2, and nesprin-2 in breast cancer. Cancer medicine. 2015 Oct.4:1547. [PubMed: 26175118]
33. Nam HS, Benezra R. High levels of Id1 expression define B1 type adult neural stem cells. Cell stem cell. 2009 Nov 6.5:515. [PubMed: 19896442]
34. Hanson PI, Roth R, Lin Y, Heuser JE. Plasma membrane deformation by circular arrays of ESCRT-III protein filaments. The Journal of cell biology. 2008 Jan 28.180:389. [PubMed: 18209100]
35. Zwerger M, et al. Myopathic lamin mutations impair nuclear stability in cells and tissue and disrupt nucleo-cytoskeletal coupling. Human molecular genetics. 2013 Jun 15.22:2335. [PubMed: 23427149]
36. Carey SP, Starchenko A, McGregor AL, Reinhart-King CA. Leading malignant cells initiate collective epithelial cell invasion in a three-dimensional heterotypic tumor spheroid model. Clinical & experimental metastasis. 2013 Jun.30:615. [PubMed: 23328900]
37. Carey SP, Kraning-Rush CM, Williams RM, Reinhart-King CA. Biophysical control of invasive tumor cell behavior by extracellular matrix microarchitecture. Biomaterials. 2012 Jun.33:4157. [PubMed: 22405848]

38. Alexander S, Koehl GE, Hirschberg M, Geissler EK, Friedl P. Dynamic imaging of cancer growth and invasion: a modified skin-fold chamber model. Histochemistry and cell biology. 2008 Dec. 130:1147. [PubMed: 18987875]

39. Jimenez AJ, et al. ESCRT machinery is required for plasma membrane repair. Science. 2014 Feb 28.343:1247136. [PubMed: 24482116]

40. Zipfel WR, et al. Live tissue intrinsic emission microscopy using multiphoton-excited native fluorescence and second harmonic generation. Proceedings of the National Academy of Sciences of the United States of America. 2003 Jun 10.100:7075. [PubMed: 12756303]

41. Needham D, Nunn RS. Elastic deformation and failure of lipid bilayer membranes containing cholesterol. Biophysical journal. 1990 Oct.58:997. [PubMed: 2249000]

42. Scheffer LL, et al. Mechanism of Ca(2)(+)-triggered ESCRT assembly and regulation of cell membrane repair. Nature communications. 2014; 5:5646.

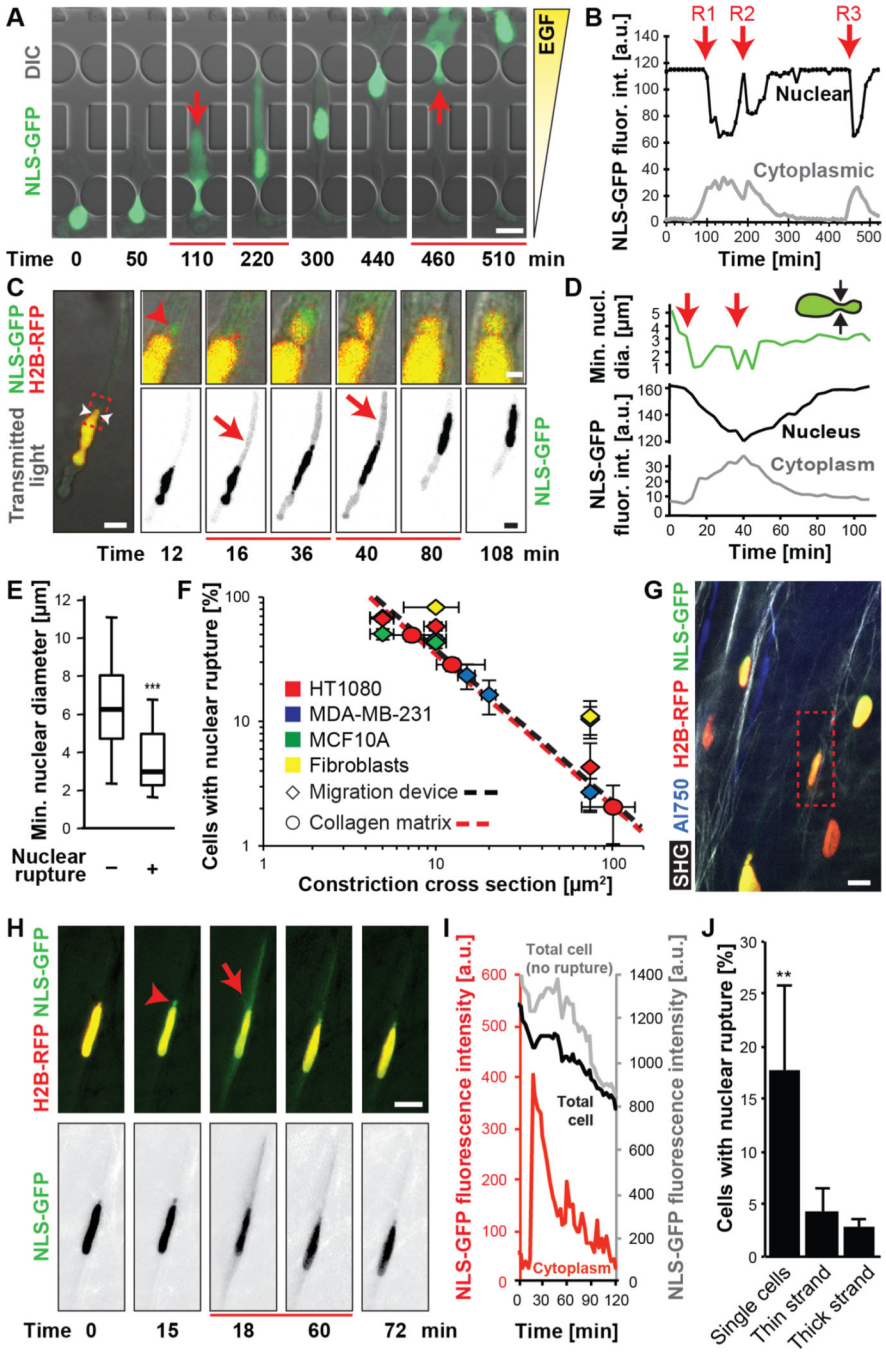

Figure 1. Nuclear rupture during migration through confining environments

(**A**) Image sequence of an MDA-MB-231 breast cancer cell that exhibited multiple NE ruptures while moving through 2 × 5 μm^2 constrictions. See also Movie S1. Here and in all other figures, red arrows and lines below frames indicate beginning and duration of NE rupture(s). Scale bar: 20 μm (**B**) Fluorescence intensity of nuclear and cytoplasmic NLS-GFP of the cell in (A), showing loss of nuclear signal and concomitant increase in cytoplasmic fluorescence upon NE rupture, followed by gradual re-import of NLS-GFP into the nucleus. R1–3 indicate NE rupture events. (**C**) NE rupture in an HT1080 fibrosarcoma

cell co-expressing NLS-GFP and fluorescently labeled histones (H2B-RFP) migrating inside a collagen matrix (2.5 mg/mL) with MMP inhibitor GM6001. See also Movie S2. Insets: close-up of nuclear bleb formation (red arrowhead). White arrowheads indicate the minimal nuclear diameter. Scale bar: 10 μm; 2 μm (insets). (**D**) Minimal nuclear diameter and nuclear and cytoplasmic NLS-GFP fluorescence intensity for the cell in (C). (**E**) Minimal nuclear diameter in rupturing and non-rupturing HT1080 cells. ***, $p < 0.001$; $n = 159$ and 62 cells, respectively. (**F**) Incidences of NE rupture as function of constriction sizes in collagen matrices (slope = –1.224; $R^2 = 0.999$) and microfluidic devices during ≈12 hour period (slope = –1.219; $R^2 = 0.974$). Regression based on HT1080 and MDA-MB-231 cells; $n =$ 55–445 cells per condition. (**G, H**) Multiphoton image of HT1080 fibrosarcoma cells 5 days after implantation into the mouse dermis. Dashed box indicates cell with NE rupture and nuclear bleb (arrowhead) shown in (H). Collagen fibers detected by second harmonic generation (SHG); blood vessels visualized by AlexaFluor-750 labeled 70 kDa-dextran. Scale bar: 20 μm. (**I**) Fluorescence intensity of cytoplasmic (red) and total (black/gray) NLS-GFP signal in rupturing (red/black) and non-rupturing (gray) cell(s) in the same field of view. (**J**) Incidence of NE rupture as function of migration mode. **, $p < 0.01$ vs. thin and thick strands; $n = 22–211$ cells. Error bars: mean ± s.e.

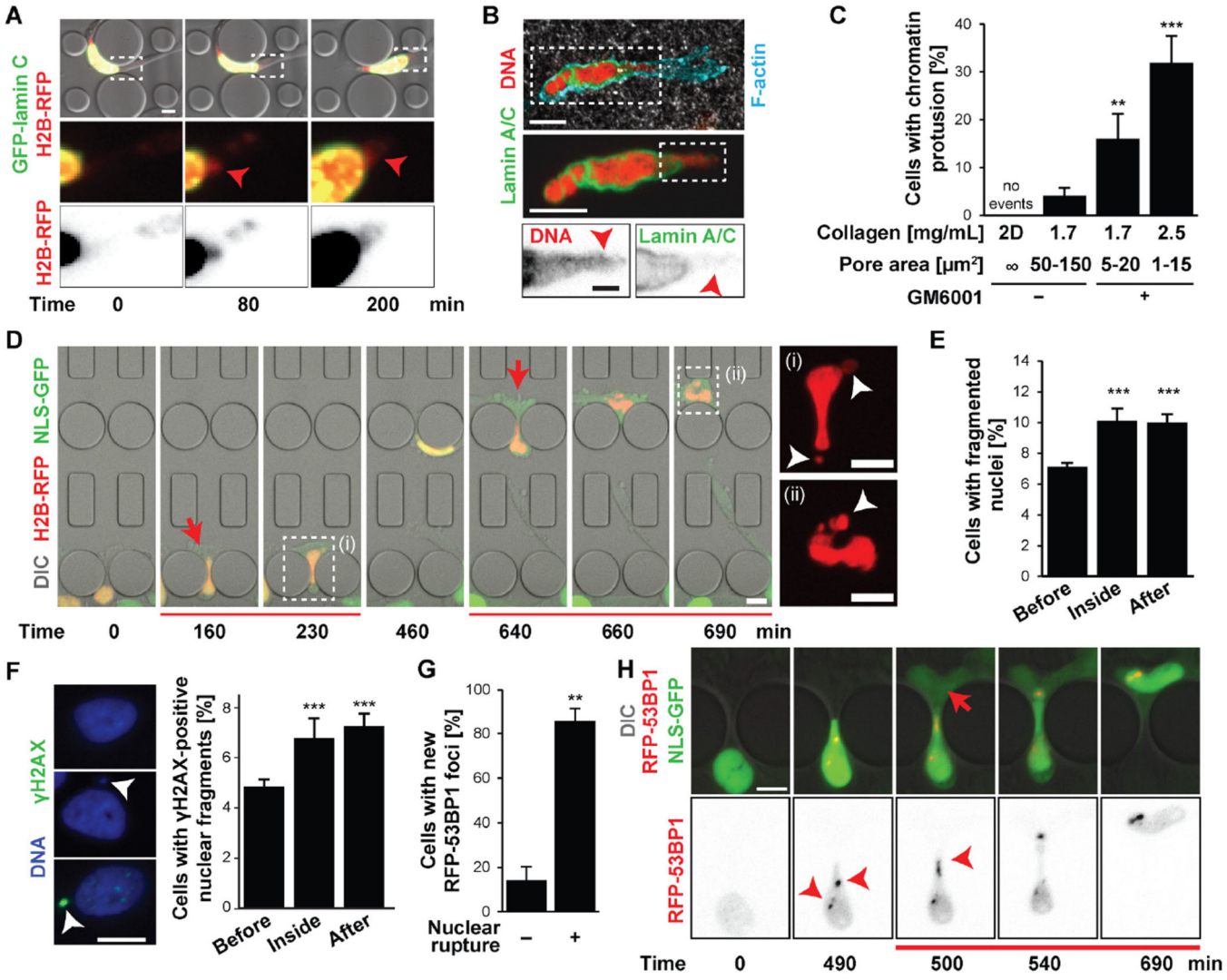

Figure 2. Confined migration leads to chromatin protrusions, nuclear fragmentation, and DNA damage

(**A**) Representative image of an MDA-MB-231 cell co-expressing GFP-lamin C and H2B-RFP developing chromatin protrusion (arrowhead) during migration through a microfluidic constriction. Scale bar: 5 µm. (**B**) HT1080 cell in a collagen matrix (2.5 mg/mL + GM6001) with chromatin protrusion (arrowheads) across the nuclear lamina, stained for lamin A/C (green), DNA (red), and F-actin (turquoise). Scale bars: 10 µm, 2 µm (bottom inset). (**C**) Percentage of cells with chromatin protrusions as a function of collagen matrix pore size. 2D, unconfined migration on glass slide. **, $p < 0.01$; ***, $p < 0.0001$; $n = 50–146$ cells per condition. (**D**) Representative image sequence of the formation of chromatin-filled nuclear membrane blebs (white arrowheads) and subsequent nuclear fragmentation in an MDA-MB-231 breast cancer cell co-expressing NLS-GFP (green) and H2B-RFP (red) during migration through consecutive 2 × 5 µm^2 constrictions. Insets are indicated by dashed lines. See also Movie S6. (**E**) Percentage of cells with fragmented nuclei before entry into constriction channel, inside the channel, and after exit. ***, $p < 0.001$; $n = 9775$, 1376, and 3072, respectively. (**F**) Example of an intact nucleus (left top), a nucleus with a small

fragment (arrowhead) (left middle), and a nucleus with a γ-H2AX-positive fragment (left bottom). Scale bar: 10 μm. Percentage of cells with γ-H2AX-positive nuclear fragments before, inside, and after migration through constriction channels (right). ***, $p < 0.001$; $n =$ 1376–3072 cells per condition. (**G**) Percentage of HT1080 cells migrating through 2 × 5 μm^2 or 1 × 5 μm^2 constrictions that formed 53BP1-RFP foci as a function of nuclear rupture. **, $p < 0.01$ $n = 35$ cells total. (**H**) Representative example of formation of 53BP1 foci (arrowheads) in U2OS cell co-expressing NLS-GFP and 53BP1-RFP during migration through 2 × 5 μm^2 constriction and NE rupture. Scale bar: 10 μm. Error bars in figure: mean ± s.e.

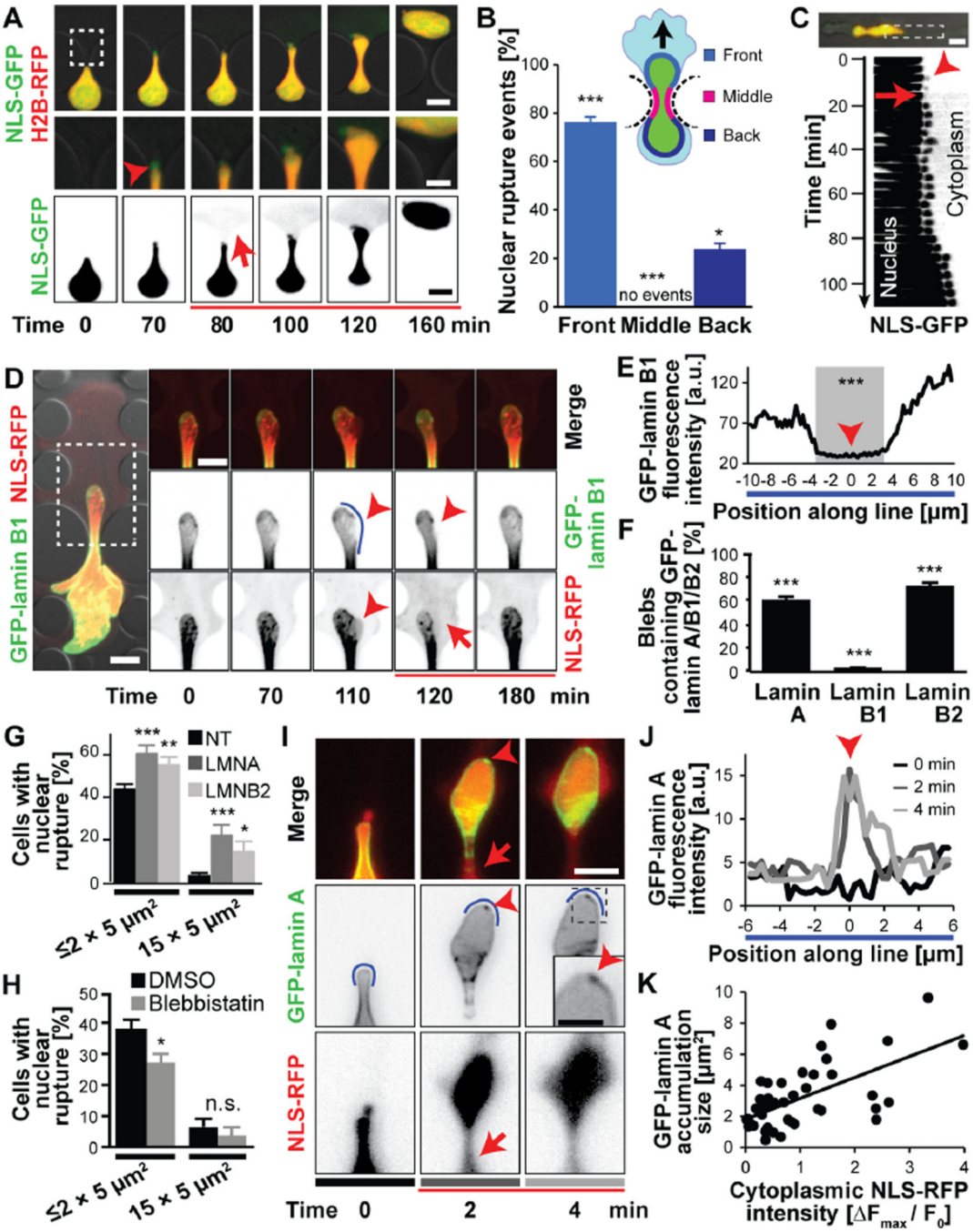

Figure 3. Molecular sequence of nuclear rupture

(**A**) Nuclear membrane bleb formation (arrowhead) and collapse upon NE rupture. Scale bars: 10 µm (top and bottom rows), 5 µm (inset). (**B**) Distribution of NE rupture sites along nuclear periphery. Regions are based on the migration direction (black arrow) and denoted in the cartoon. $n = 352$ cells; *, $p < 0.05$; ***, $p < 0.001$; all comparisons relative to the hypothetical uniform distribution of 33%. (**C**) Kymograph of nuclear bleb formation (arrowhead) and collapse during subsequent NE rupture, corresponding to the image sequence in Fig. 1C. (**D**) Nuclear membrane blebs formed at sites of low GFP-lamin B1

intensity and were devoid of GFP-lamin B1 (arrowheads). Intensity along the blue line is quantified in panel E. Representative cell out of 178 cells observed. (**E**) GFP-lamin B1 fluorescence intensity profile. The gray area indicates the section where the nuclear bleb forms. ***, $p < 0.0001$; comparing values inside versus outside gray area. (**F**) Percentage of nuclear blebs containing detectable amounts of either lamin A, B1, B2. ***, $p < 0.001$; compared to the expected value of 100% for the primary nucleus; $n = 178–199$ cells per condition. (**G**) Incidence of NE rupture after siRNA treatment against lamins A/C, lamin B2, or non-target (NT) control. *, $p < 0.05$; **, $p < 0.01$; ***, $p < 0.001$; $n = 384$, 150, and 163 cells for constrictions ≤ 2 × 5 μm^2; $n = 166$, 68, and 49 for 15 × 5 μm^2 constrictions. (**H**) Blebbistatin treatment reduced NE rupture incidence during migration in constriction channels, but not in 15 × 5 μm^2 control channels. *, $p < 0.05$; $n = 286$ and 194 for constrictions ≤ 2 × 5 μm^2; $n = 122$, and 54 for cells in 15 × 5 μm^2 constrictions. (**I**) GFP-lamin A accumulated at sites of NE rupture, forming ‘lamin scars’ (arrowheads). Grey bars under images correspond to line profiles at different times in (J). Scale bar: 10 μm. (**J**) GFP-lamin A signal intensity along a section of the nuclear rim (blue line in panel I). (**K**) GFP-lamin A accumulation increases with the severity of NE rupture. $p < 0.0001$; $n = 46$ cells (slope = 1.345, $R^2 = 0.3945$). Error bars in figure: mean ± s.e.

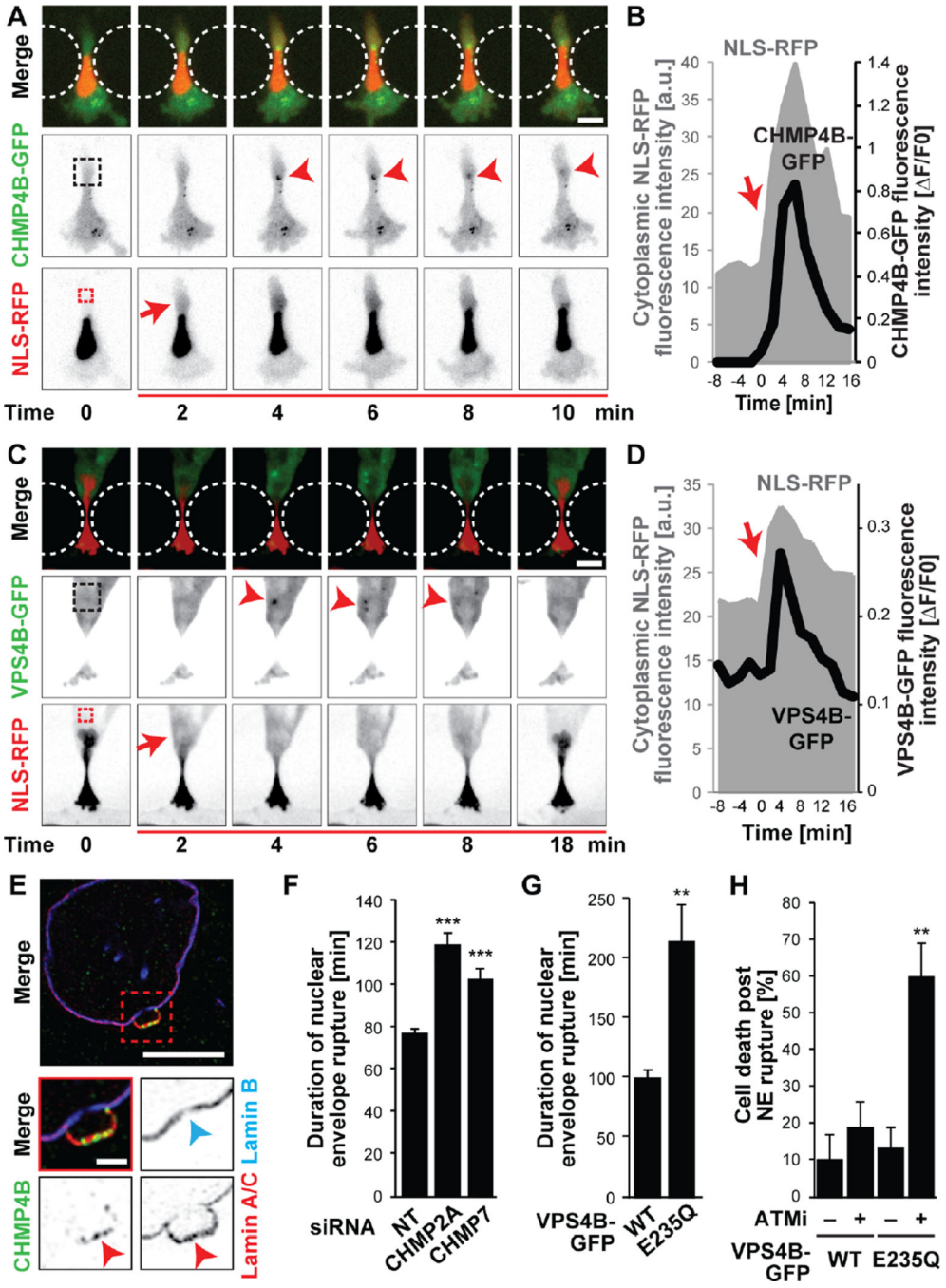

Figure 4. ESCRT-III mediates nuclear envelope repair

(**A**) CHMP4B-GFP was transiently recruited to the site of nuclear membrane damage (arrowhead). See also Movie S7. Dashed boxes indicate areas used for measurements in (B). Representative sequence from 12 HT1080 cells total. Scale bar: 10 μm. (**B**) CHMP4B-GFP fluorescence intensity at rupture site (black), normalized to pre-rupture intensity, increased following NE rupture, indicated by increase in cytoplasmic RFP-NLS signal (grey). Red arrow indicates time of NE rupture. (**C**) Recruitment of VPS4B-GFP to sites of NE rupture (arrowhead) in an MDA-MB-231 cell. Dashed boxes indicate areas used for measurements

in (D). Representative example from 18 cells total. Scale bar: 10 μm. (**D**) VPS4B-GFP fluorescence intensity in the cytoplasm (black) increased rapidly following NE rupture, detected by increase in cytoplasmic RFP-NLS signal (grey). Red arrow indicates time of NE rupture. (**E**) Representative super-resolution image (from 12 cells total) of endogenous CHMP4B accumulation at NE rupture site. Lamin A/C accumulation confirmed rupture site (red arrowhead). Blue arrowhead indicates decreased lamin B intensity at the base of the bleb. Scale bars: 5 μm and 1 μm (inset). (**F**) siRNA-mediated depletion of ESCRT-III proteins CHMP7 and CHMP2A in HT1080 cells resulted in an increased duration of NLS-GFP in the cytoplasm after migration induced NE rupture compared to non-target (NT) controls. ***, $p < 0.001$; $n = 137$ and 107, respectively. (**G**) Expression of the dominant-negative mutant VPS4B^{E235Q}-GFP increased the duration of NLS-GFP in the cytoplasm after migration induced NE rupture in HT1080 cells, indicating impaired nuclear membrane repair. **, $p < 0.005$; $n = 17$ and 10, respectively. (**H**) Percentage of HT1080 cells dying after migration induced NE rupture, in the absence or presence of inhibition of ESCRT-III by dominant-negative VPS4B^{E235Q}-GFP and/or DNA repair with the ATM inhibitor KU-55933 (ATMi). **, $p < 0.01$; $n = 20, 32, 38, 30$, respectively, compared to WT with ATMi and E235Q without ATMi. Error bars in figure: mean ± s.e.m.